Journal of Nuclear Medicine, published on May 28, 2021 as doi:10.2967/jnumed.121.262134

Detecting fibroblast activation proteins in lymphoma using ^{68}Ga-FAPI PET/CT

Running Title: ^{68}Ga-FAPI PET/CT in lymphoma

Xiao Jin[*1], Maomao Wei[*1], Shuailiang Wang[*1], Guochang Wang[*1], Yumei Lai [2], Yunfei Shi [2], Yan Zhang [1], Zhi Yang [1], Xuejuan Wang [1]

Affiliations:

[1] Key Laboratory of Carcinogenesis and Translational Research (Ministry of Education/Beijing), NMPA Key Laboratory for Research and Evaluation of Radiopharmaceuticals (National Medical Products Administration), Department of Nuclear Medicine, Peking University Cancer Hospital & Institute, Beijing, 100142, China

[2] Key Laboratory of Carcinogenesis and Translational Research (Ministry of Education), Department of Pathology, Peking University Cancer Hospital & Institute, Beijing 100142, China

[*]Contributed equally to this work.

For correspondence or reprints contact:

Xuejuan Wang

Department of Nuclear Medicine, Peking University Cancer Hospital & Institute

52 Fucheng Road, Haidian, Beijing, China, 100142

Email: xuejuan_wang@hotmail.com

Telephone: +86 10 88196363; Fax: +86 10 88196196

ORCID-ID: 0000-0003-3648-5874

First authors:

Xiao Jin and Guochang Wang are Residents at the Department of Nuclear Medicine, Peking University Cancer Hospital & Institute, Beijing, China.

Maomao Wei and Shuailiang Wang are students at the Department of Nuclear Medicine, Peking University Cancer Hospital & Institute, Beijing, China.

Declarations:

Funding: This work was financially supported by the National Natural Science Foundation of China (no. 82071957), Beijing Hospitals Authority Clinical Medicine Development of special funding support (code: XMLX202120), and Capital's Funds for Health Improvement and Research (no. 2018-2-1024).

Conflicts of interest: The authors declare no potential conflicts of interest.

Ethics approval: The study was approved by the Institutional Review Board of Beijing Cancer Hospital (no. 2019KT95) and registered in ClinicalTrials.gov (NCT04367948).

Word Count: 4696 words

ABSTRACT

Purpose: Cancer-associated fibroblasts (CAFs) that overexpress fibroblast activation protein (FAP) are enriched in many epithelial carcinomas and in hematological neoplasms. Positron emission tomography/computed tomography (PET/CT) with radiolabeled FAP inhibitor (FAPI) is a new diagnostic tool for visualizing the tumor stroma. This prospective study aimed to profile FAPs in different subtypes of lymphomas and explore the potential utility of ^{68}Ga-FAPI PET/CT in lymphomas.

Methods: In this prospective study, we recruited 73 lymphoma patients who underwent ^{68}Ga-FAPI PET/CT and recorded and measured semiquantitative parameters and ratios of their scan results. FAPI expression was assessed by immunochemistry in samples obtained from 22 of the lymphoma patients.

Results: We evaluated 11 patients with Hodgkin lymphoma (HL) and 62 with non-Hodgkin lymphoma (NHL). Significantly elevated FAP uptake was observed in HL lesions, correlating with the intensity of FAP immunostaining (score, 3+). A positive association was found between the corresponding clinical classification of NHL and the ^{68}Ga-FAPI uptake activity of the lesion. Aggressive NHL lesions, with moderate-to-strong FAP immunostaining (score, 2+ to 3+), exhibited intense to moderate ^{68}Ga-FAPI uptake. Indolent NHL lesions showed weak FAP staining and mild to moderate ^{68}Ga-FAPI uptake. No statistically significant correlation emerged between the sum of the product of the diameters and the corresponding maximum standardized uptake value (P = 0.424). The tumor-to-liver ratios were 6.26 ± 4.17 in indolent NHL and > 9 in other subtypes.

Conclusion: ^{68}Ga-FAPI imaging can be used to detect FAP expression in lymphoma lesions and may be an alternate method for characterizing lymphoma profiles.

Key words: ^{68}Ga-FAPI PET, lymphoma, cancer-associated fibroblasts, fibroblast activation protein, tumor stroma

INTRODUCTION

Lymphomas are a heterogeneous group of malignancies arising from lymphocytes and typically involve lymphoid organs. They account for approximately 3.5% of new malignant cases worldwide, with B-cell lymphomas (BCLs) and Hodgkin lymphoma (HL) accounting for 80% and 10% of all lymphoma cases, respectively. Lymphoma pathogenesis is well understood, and there is increasing focus on nonmalignant cells residing in the tumor, primarily immune and stromal cells, which constitute the so-called tumor microenvironment (*1*).

Recent studies have suggested that the outcome of patients with lymphoma is entwined with the remarkable heterogeneity of both the malignant clone and the cellular/extracellular microenvironment and unveiled fibroblasts in the microenvironment that might exhibit both a pro- and antitumorigenic phenotype (*2,3*). A stromal gene signature representing fibroblasts has been shown to correlate with poor survival in carcinomas, including breast, ovarian, pancreatic, and colorectal cancer. Paradoxically, a closely related gene signature has been associated with good survival in BCLs (*4,5*). This contradictory result has generated lots of interest and effort in elucidating fibroblast-mediated effects. Even though these studies indicated that stromal signatures of BCLs could predict survival, they were clinically restrained by the lack of robust and reproducible biomarkers (*6,7*). Additionally, to support histopathological and genic evidence, the tumor stroma needs to be visualized and monitored, and imaging is an essential aspect of the diagnostic workup.

Nonhematopoietic ($CD45^{-}$) tumor stroma in lymphoid tissues comprise cells of

mesenchymal origin and vascular endothelial cells (*8*). Cancer-associated fibroblasts (CAFs) belong to the $CD45^{-}$-reprogrammed myelofibroblastic network and play a crucial role in the development and progression of solid tumors (*9*). CAFs and activated fibroblasts selectively overexpress a growth factor, fibroblast activation protein (FAP). Molecular positron emission tomography/computed tomography (PET/CT) imaging with radiolabeled FAP inhibitor (FAPI) has been evaluated in various diseases, but not in lymphoma (*10,11*). Recently, we incidentally found a mild ^{68}Ga-FAPI uptake in a primary gastric diffuse large BCL (DLBCL) lesion. Thus, we hypothesize that CAFs in lymphoma could be imaged using ^{68}Ga-FAPI PET/CT (*12*).

The aim of this prospective study was to identify FAPs with ^{68}Ga-FAPI-04 PET/CT in different subtypes of lymphomas (especially T-cell lymphoma), quantify ^{68}Ga-FAPI-04 accumulations in nodal and extranodal lesions, and explore the potential utility of ^{68}Ga-FAPI-04 PET/CT in lymphomas.

PATIENTS AND METHODS

Patients

This prospective study was approved by the Institutional Review Board of our hospital (no. 2019KT95) and registered with ClinicalTrials.gov (NCT04367948). Written informed consent was obtained from the patients for receiving ^{68}Ga-FAPI PET/CT examinations and the publication of their anonymous data accompanying the imaging results. Study enrollment was performed from December 2019 to August 2020. The patient inclusion criteria were (i) pathologically diagnosed as lymphoma,

(ii) aged 18 – 75 years, (iii) expected survival ≥ 12 weeks, and (iv) minimum one target lesion with ^{68}Ga-FAPI uptake. The exclusion criteria were (i) severe liver or kidney dysfunction, (ii) pregnancy or lactation, (iii) inability to lie on the scanner bed for less than 0.5 h, and (iv) inability or unwillingness of the patient or legal representative to provide written informed consent. The final study cohort comprised 73 patients with lymphoma. The study flowchart of patient enrollment is presented in Supplement 1.

Radiopharmaceuticals

Synthesis and radiolabeling of ^{68}Ga-FAPI-04 were performed as previously described. Briefly, ^{68}Ga was chelated after pH adjustment with sodium acetate. Then, a reaction mixture of 25 μg (28.6 nmol) FAPI-04 and 1.7 GBq ^{68}Ga solution was heated to 100 °C for 10 min. Next, the reaction solution was diluted to 5 ml and passed through a preconditioned Sep-Pak C18 Plus Light Cartridge (Waters), and the cartridge was eluted with 0.5 ml 75% ethanol to obtain the final product. Quality control of the radiosynthesis was performed by ultraviolet and radio-high-performance liquid chromatography, and the radiochemical purity was >95%. The ^{68}Ga-FAPI injections were filtered through a 0.22 μm Millex-LG filter (EMD Millipore) before clinical use.

PET/CT Imaging

The radiopharmaceutical was administrated intravenously at a dose of 1.8–2.2

MBq/kg. At approximately 60 ± 10 min post injection, a torso acquisition (n = 52) commenced in 6–8 bed positions (1 min/bed) using a hybrid system (PHILIPS Gemini TF PET/CT Scanner) that covered from the base of the skull to the upper thigh. Noncontrast-enhanced CT was performed using 100 mA modulation, 120 kV, and a slice thickness of 3 mm for attenuation correction and anatomical localization purposes. The dedicated head acquisition was separately performed in one bed position (8–10 min/bed). The acquisitions from the top of the skull to the upper thigh or the tip of the toes were performed in the remaining 21 patients. The emission data were corrected for random, scatter, and decay. The data were reconstructed using the ordered subset expectation maximum algorithm to obtain coronal, sagittal, and cross-sectional PET and PET/CT fusion images. The total scan time was approximately 19 min. The patients were asked to self-report any abnormalities at 30 min after the PET/CT scans.

Image Interpretation

Three experienced nuclear physicians were assigned to independently interpret each patient's PET images with knowledge of the clinicopathological data on a PHILIPS EBW workstation. The presence and sites of lymphoma involvement and the intensity of the ^{68}Ga-FAPI uptake in the lesions were recorded for each PET scan. Increased radioactivity compared with the background uptake was considered positive and was measured and calculated via the region of interest technique. Any discordant results were resolved by consensus. Up to six of the largest and/or highest SUV_{max}

lymphoma lesions were identified from different body regions for each PET/CT scan. The product of the diameters was calculated by multiplying the longest diameter by the shortest diameter for each lesion. Then, the products of the diameters were added to assess the sum of products of the diameters (SPD), which was representative of the patient's overall disease burden. The nonspecific background in the liver was quantified with a circular 2-cm-diameter sphere and the tumor-to-liver ratio was calculated.

Immunohistochemistry

FAP expression in lymphoma lesions was determined using postsurgical histology samples from seven patients and biopsy samples from 15 patients via immunohistochemistry performed as per a previous report. Before immunohistochemistry staining, the tissue sections were stained with hematoxylin and eosin and reviewed by two experienced pathologists. FAP was detected using a rabbit monoclonal antibody against FAP (BM5121; Boster). Briefly, formalin-fixed, paraffin-embedded blocks were cut into 4-μm-thick sections, deparaffinized in xylene, and rehydrated. Antigen retrieval was performed using EDTA (pH 8.0; Santa Cruz Biotechnology) in a pressure cooker for 3 min. Then, the sections were incubated in 3% H_2O_2 solution for 10 min at room temperature to block endogenous peroxidase activity. Immunohistochemistry was performed with anti-FAP antibody at a dilution of 1:400 for 12 h at 4 °C. Subsequently, anti-rabbit IgG-horseradish peroxidase-linked secondary antibody was applied for 30 min at 37 °C. Then, the sections were

developed with 3,3′-diaminobenzidine tetrahydrochloride. Mayer's hematoxylin was applied for 5 min as a counterstain. Photographs of representative fields were taken using an N-Achroplan objective (ZEISS). The FAP expression was assessed visually and quantitatively. Stromal cell staining was scored as 0 (absence of FAP immunostaining), 1+ (weak FAP staining in <10% of stromal cells), 2+ (positive FAP immunostaining in 10%–50% of stromal cells), and 3+ (moderate to strong FAP immunostaining in >50% of stromal cells) (*13*).

Statistical Analysis

All statistical analyses were conducted using SPSS 20.0 software (IBM Corp.). SUVs were presented as the mean ± standard deviation. The Kolmogorov–Smirnov test was used to determine whether the data were normally distributed. Comparisons between the average maximum standardized uptake value (SUV_{max}) were made using the *t*-test or Mann–Whitney U test. The correlation between SUV_{max} and histological subtypes was evaluated by the Pearson correlation coefficient. A *P*-value <0.05 was considered statistically significant.

RESULTS

Patient Characteristics

We enrolled 73 patients (36 females and 37 males; age, 51.6 ± 14.2 years; range, 21–74 years) in our study. Of them, 48 had newly diagnosed lymphoma, 17 had progressive disease, and eight had relapses. Non-Hodgkin lymphoma (NHL; *n* = 62,

84.93%) was the most prevalent pathological subtype, including DLBCL (*n* = 34, 46.57%), follicular lymphoma (*n* = 9, 12.33%), extranodal NK/T-cell lymphoma (*n* = 5, 6.85%), angioimmunoblastic T-cell lymphoma (*n* = 4, 5.48%), primary mediastinal large BCL (*n* = 2, 2.74%), and mucosa-associated lymphoid tissue (MALT) lymphoma (*n* = 2, 2.74%). The other enrolled subtypes had one case each. Fifteen cases (20.55%) only involved lymph nodes, and 19 (26.02%) were primary extranodal lymphomas (Table 1).

Quantifying ^{68}Ga-FAPI-04 Uptake in Lymphoma Lesions

The ^{68}Ga-FAPI-04 PET/CT scans were visually positive for detecting lymphoma in 72/73 (98.6%) patients because of the low background, except a patient with primary gastric MALT lymphoma. The average SUV_{max}, median SUV_{max}, and SUV_{max} range of the lymphoma lesions was 9.46 ± 4.61, 8.9, and 1.7–23.3, respectively. The average SUV_{max} of the initial assessment, progressed, and relapsed group was 9.74 ± 4.88, 9.37 ± 5.03, and 8.35 ± 2.57, respectively (P = 0.769). The overall SUV_{max} (7.98 ± 4.39 vs. 8.49 ± 4.45), median SUV_{max} (7.3 vs. 7.5) and SUV_{max} range (1.7–23.0 vs. 1.8–21.0) of ^{68}Ga-FAPI in nodal and extranodal lesions did not differ (P > 0.05). Similar results were found in various histological subtypes (P > 0.05) (Table 2).

The lymph node sizes and SPDs in different histological subtypes are shown in Table 3. The mean SPD, median SPD, and SPD range of lymphoma lesions were 34.22 ± 34.46, 25.54, and 2.10–229.49, respectively. No statistically significant correlation emerged between the SPD and corresponding SUV_{max} (r = 0.107, P =

0.424).

All tumor entities exhibited a high interindividual and intralesional SUV variation (Figure 1 & graphical abstract). The highest average SUV_{max} (>10) was found in primary mediastinal large BCL, Burkitt lymphoma, HL, and DLBCL. The lowest ^{68}Ga-FAPI intensity (average SUV_{max} <5) was observed in MALT lymphoma. Other subtypes showed moderate ^{68}Ga-FAPI uptake (average SUV_{max} 5–10). No statistically significant difference was found between the SUV_{max} of HL (10.74 ± 3.95) and NHL (9.23 ± 4.71) (P = 0.323). The SUV_{max} values of BCLs (9.97 ± 4.68) were significantly higher than those of T-cell lymphomas (7.19 ± 1.73) (P = 0.002). Figure 2 exhibits various extranodal sites in the enrolled patients.

According to the clinical classification for NHL, the average SUV_{max} of ^{68}Ga-FAPI in aggressive (n = 50) lymphoma was significantly higher than in indolent (n = 12) lesions (9.97 ± 4.68 vs. 6.16 ± 3.57; P= 0.008). Correlation analysis revealed a moderate correlation between the clinical classification and SUV_{max} (r = 0.338, P = 0.007). Because of the low background activity (average SUV_{mean} of liver: 1.11 ± 0.36), the tumor-to-liver ratios were 9.89 ± 6.08, 10.03 ± 5.12, and 6.26 ± 4.17 in HL, aggressive NHL, and indolent NHL, respectively.

Immunohistochemistry

To further characterize FAP as a target structure within lymphoma, we performed FAP-immunohistochemistry in 22 of the included cases. There were four patients with HL and 18 patients with NHL (9 DLBCL, 2 extranodal NK/T-cell lymphoma, 1

angioimmunoblastic T-cell lymphoma, 1 mantle cell lymphoma, 3 follicular lymphoma, 1 MALT lymphoma, and 1 chronic lymphocytic leukemia/small lymphocytic lymphoma [CLL/SLL]).

The pathological examinations showed intense FAP expression (score, 3+) in all HL lesions (4/4). For NHL, 7 of 12 aggressive lesions scored 3+ for FAP immunostaining, 4 of 5 indolent lesions showed weak FAP expression (score, 1+), and 5 of 9 DLBCL lesions overexpressed FAP (score, 3+). Weak FAP expression (score, 1+) was detected in MALT lymphoma lesions. Surprisingly, CLL/SLL lesions showed moderate FAP expression (score, 2+). Furthermore, lesions with intense FAP expression exhibited higher SUV_{max} values compared with lesions that scored 1+, and a statistically significant correlation was unmasked between the SUV_{max} of lymphoma lesions and FAP expression ($b = 0.551$, $P < 0.001$).Figure 3 shows representative examples of the FAP immunostaining results.

DISCUSSION

The most crucial contribution of our study is the first visualization of FAPs in malignant lymphoid tumors, particularly in T-cell lymphomas. Moreover, we quantified the accumulation of ^{68}Ga-FAPI ligand in different subtypes of lymphoma lesions.

Fibroblastic reticular cells are specialized myofibroblasts that create the lymph node skeleton with its conduit system (*14*). Malignant cells recruit and re-educate their surrounding cells to establish a tumor-supportive milieu that also affects the

biology and function of fibroblastic reticular cells. Once reprogrammed to CAFs, they can induce extracellular matrix remodeling (*15*). There is increasing evidence that CAFs can potentially regulate tumor progression in hematological neoplasms. Lenz et al. *(3)* and Haro et al. (*4*) reported that the stromal-1 gene signature was associated with good survival in patients with DLBCL and several other BCLs. Paradoxically, Bankov et al. *(7)* and Aronovich et al. (*16*) demonstrated that fibroblasts in classic HL and mycosis fungoides promoted tumor cell migration and drug resistance. These conflicting results indicate that there is still much to learn about the biological and clinical significance of CAFs in different lymphoma subtypes. Thus, a new strategy is necessary to depict tumor–stroma interaction in lymphoma that does not involve visualization using morphological or metabolic imaging.

Biologically, ^{68}Ga-FAPI PET/CT is an excellent imaging modality to visualize FAP expression in the tumor stroma (*10,17*). The majority of false-positive results occur in wound healing and inflammatory or fibrosis conditions caused by the activation, proliferation, and accumulation of fibroblasts (*11*). Although clinical evaluations of ^{68}Ga/^{18}F-FAPI PET have been performed in a spectrum of cancers, there are none involving lymphomas. In our study, 72 lymphoma patients referred for ^{68}Ga-FAPI PET imaging showed FAPI-positive lesions in most of subtypes of lymphoma, including both BCLs and T-cell lymphomas, except a patient with MALT lymphoma.

Since the origin, number, and distribution of FAP-expressing CAFs as well as the number of FAP molecules per cell may differ in tumors, we expect varying tumor

uptake as well as variations in the intratumoral tracer distribution. HL, especially the nodular sclerosing subtype of classic HL is characterized by fibroblast proliferation in the tumor microenvironment, leading to fibrotic bands surrounding the lymphoma infiltrate. In our study, we found intense FAP immunostaining and significantly elevated FAPI uptake in HL lesions. Regarding NHL, there was a positive association between the clinical classification of NHL and ^{68}Ga-FAPI uptake activity of the lesion in PET/CT imaging. Aggressive NHL, especially DLBCL, exhibited intermediate-to-intense ^{68}Ga-FAPI uptake and showed moderate to strong FAP immunostaining. These results were consistent with Haro's findings, who reported a high proportion of CAFs in B-cells lymphomas via a stromal gene signature analysis (*4*). Less common aggressive NHL subtypes, such as mantle cell lymphoma, B lymphoblastic leukemia/lymphoma, primary cutaneous anaplastic large-cell lymphoma, and angioimmunoblastic T-cell lymphoma, with moderate FAP expression (score, 2+), exhibited moderate ^{68}Ga-FAPI avidities. Surprisingly, we noted that follicular lymphoma, which showed the lowest desmoplastic reaction by histopathology, had intermediate ^{68}Ga-FAPI uptake (SUV_{max}: 6.69±3.85). MALT lymphoma, which showed weak FAP staining, exhibited mild ^{68}Ga-FAPI uptake, as expected. However, we did not expect that T-cell lymphoma would accumulate less ^{68}Ga-FAPI, even though the lesions expressed moderate to intense FAP expression.

Because of the very low background activity for ^{68}Ga-FAPI, especially in the brain, liver, and peritoneal cavity, the high tumor-to-background ratios resulted in high contrast ratios of lymphoma lesions, particularly in the brain, liver, and

oropharynx. These may be advantageous for the detection of cerebral, hepatic, or oropharyngeal involvement. As previous studies have reported, we also easily identified a DLBCL lesion in the left temporal lobe in our study.

Because of the limitations of this report, such as a heterogeneous patient collective and a low case number for some subtypes, further studies are necessary. Furthermore, due to the lack of follow-up, analysis of the long-term prognosis regarding disease-free and overall survival is currently unfeasible. Therefore, larger prospective clinical studies are needed for further evaluation.

CONCLUSION

Our study results showed that ^{68}Ga-FAPI PET/CT is an extremely useful technique for profiling FAP expression status in lymphoma lesions. HL and aggressive NHL may possess more CAFs in tumor stroma compared with indolent disease.

KEY POINTS

QUESTION: Can ^{68}Ga-FAPI PET/CT detect FAPs in lymphoma?

PERTINENT FINDINGS: In this prospective study of 73 lymphoma patients, we found that ^{68}Ga-FAPI PET/CT could be used to profile FAP expression status in lymphoma lesions. Furthermore, HL and aggressive NHL may possess more FAPs in tumor stroma compared with indolent disease.

IMPLICATIONS FOR PATIENT CARE: FAPI imaging may be an alternate method for characterizing lymphoma profiles.

REFERENCES

1. Höpken UE, Rehm A. Targeting the tumor microenvironment of leukemia andlymphoma. *Trends Cancer*. 2019;5:351–364.

2. Augsten M. Cancer-associated fibroblasts as another polarized cell type of thetumor microenvironment. *Front Oncol*. 2014;4:62.

3. Lenz G, Wright G, Dave SS, et al. Stromal gene signatures in large-B-cell lymphomas. *N Engl J Med.* 2008;359:2313–2323.

4. Haro M, Orsulic S. A paradoxical correlation of cancer-associated fibroblasts with survival outcomes in B-cell lymphomas and carcinomas. *Front Cell Dev Biol*. 2018;6:98.

5. Ciavarella S, Vegliante MC, Fabbri M, et al. Dissection of DLBCL microenvironment provides a gene expression-based predictor of survival applicable to formalin-fixed paraffin-embedded tissue. *Ann Oncol*. 2018;29:2363–2370.

6. Staiger AM, Duppel J, Dengler MA, et al. An analysis of the role of follicular lymphoma-associated fibroblasts to promote tumor cell viability following drug-induced apoptosis. *Leuk Lymphoma*. 2017;58:1922–1930.

7. Bankov K, Döring C, Ustaszewski A, et al. Fibroblasts in nodular sclerosing classical Hodgkin lymphoma are defined by a specific phenotype and protect tumor cells from brentuximab-vedotin induced injury. *Cancers (Basel)*. 2019;11:1687.

8. Roozendaal R, Mebius RE. Stromal cell-immune cell interactions. *Annu Rev Immunol*. 2011;29:23–43.

9. Kalluri R. The biology and function of fibroblasts in cancer. *Nat Rev Cancer*. 2016;16:582–598.

10. Kratochwil C, Flechsig P, Lindner T, et al. ^{68}Ga-FAPI PET/CT: tracer uptake in28 different kinds of cancer. *J Nucl Med*. 2019;60:801–805.

11. Altmann A, Haberkorn U, Siveke J. The latest developments in imaging of fibroblast activation protein. *J Nucl Med*. 2021;62:160–167.

12. Wang G, Jin X, Zhu H, et al. ^{68}Ga-NOTA-FAPI-04 PET/CT in a patient with primary gastric diffuse large B cell lymphoma: comparisons with [^{18}F] FDG PET/CT. *Eur J Nucl Med Mol Imaging*. 2021;48:647–648.

13. Serfling S, Zhi Y, Schirbel A, et al. Improved cancer detection in Waldeyer's tonsillar ring by ^{68}Ga-FAPI PET/CT imaging. *Eur J Nucl Med Mol Imaging*. October 15, 2020 [Epub ahead of print].

14. Roozendaal R, Mebius RE, Kraal G. The conduit system of the lymph node. *Int Immunol*. 2008;20:1483–1487.

15. Öhlund D, Elyada E, Tuveson D. Fibroblast heterogeneity in the cancer wound. *J Exp Med*. 2014;211:1503–1523.

16. Aronovich A, Moyal L, Gorovitz B, et al. Cancer-associated fibroblasts in mycosis fungoides promote tumor cell migration and drug resistance through CXCL12/CXCR4. *J Invest Dermatol*. 2021;141:619–627.e2.

17. Lindner T, Loktev A, Altmann A, et al. Development of quinoline-based theranostic ligands for the targeting of fibroblast activation protein. *J Nucl Med*. 2018;59:1415–1422.

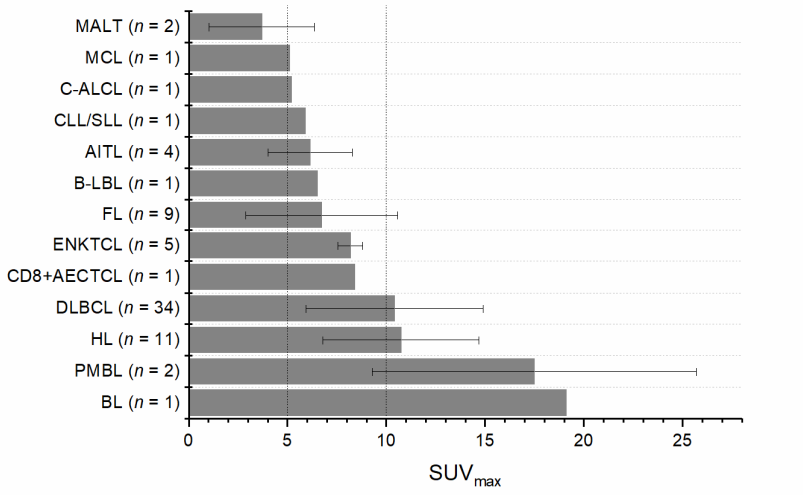

FIGURE 1 Average SUV_{max} of ^{68}Ga-FAPI PET/CT in various histological subtypes. MALT, mucosa-associated lymphoid tissue; MCL, mantle cell lymphoma; C-ALCL, primary cutaneous anaplastic large-cell lymphoma; CLL/SLL, chronic lymphocytic leukemia/small lymphocytic lymphoma; AITL, angioimmunoblastic T-cell lymphoma; B-LBL, B lymphoblastic leukemia/lymphoma; FL, follicular lymphoma; ENKTCL, extranodal NK/T-cell lymphoma; $CD8^+$ AECTCL, cutaneous $CD8^+$ aggressive epidermotropic cytotoxic T-cell lymphoma; DLBCL, diffuse large B-cell lymphoma; HL, Hodgkin lymphoma; PMBL, primary mediastinal large B-cell lymphoma; BL, Burkitt lymphoma.

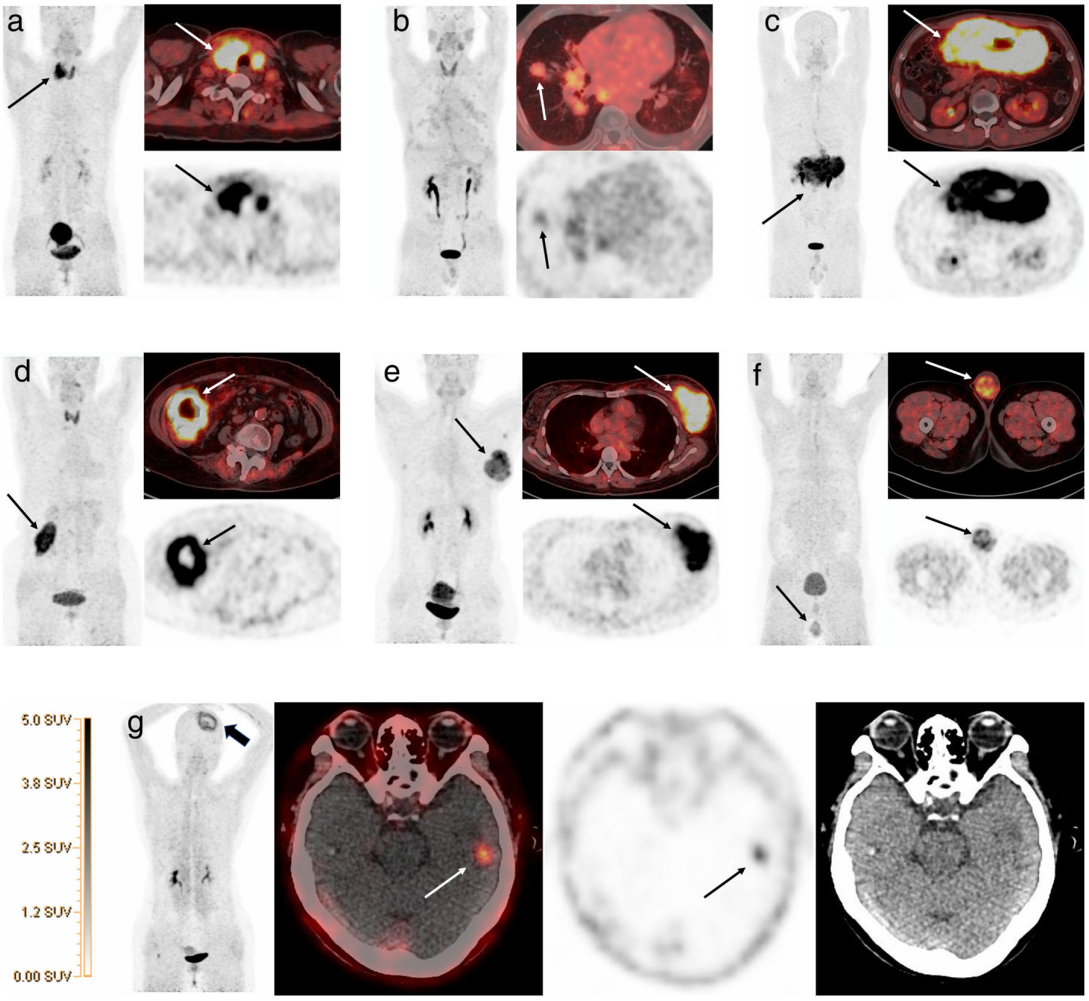

FIGURE 2. Maximum intensity projections, axial ^{68}Ga-FAPI PET, and fused images of various extranodal sites in the enrolled patients. (a), Primary thyroid Burkitt lymphoma (arrow). (b), Hodgkin lymphoma with lung involvement (arrow). (c), Primary gastric diffuse large B-cell lymphoma (DLBCL, arrow). (d), Ileum DLBCL (arrow). (e), Left breast DLBCL (arrow). (f), Left testicle DLBCL (arrow). (g), Left temporal lobe DLBCL lesion (arrow) after left frontal lymphoma resection (thick arrow).

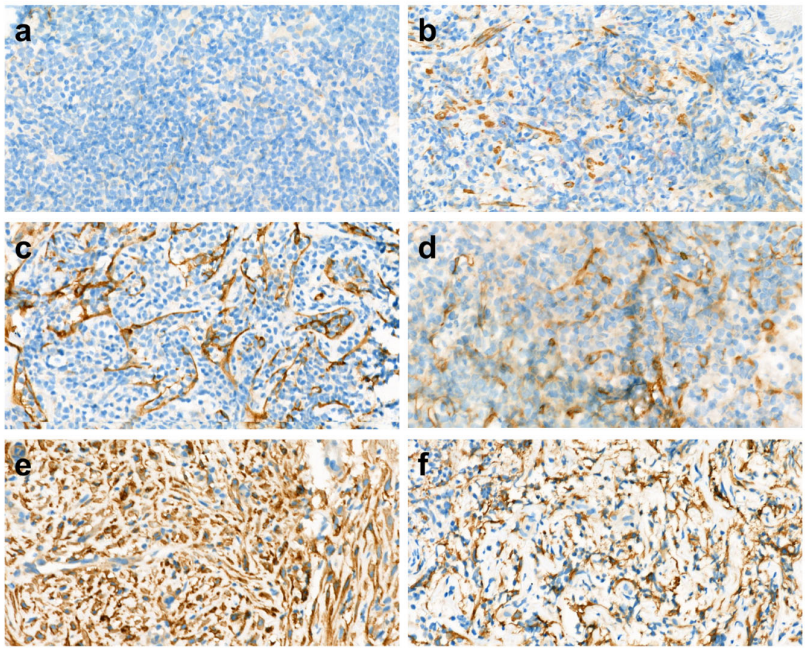

FIGURE3. FAP-immunohistochemistry of six exemplary cases of lymphoma. (a) Follicular lymphoma and (b) mucosa-associated lymphoid tissue with mild stromal FAP expression and FAP-negative neoplastic cells. (c) Chronic lymphocytic leukemia/small lymphocytic lymphoma and (d) diffuse large B-cell lymphoma with moderate stromal FAP expression. (e) Diffuse large B-cell lymphoma and (f) HL with intense stromal FAP expression.

GRAPHICAL ABSTRACT

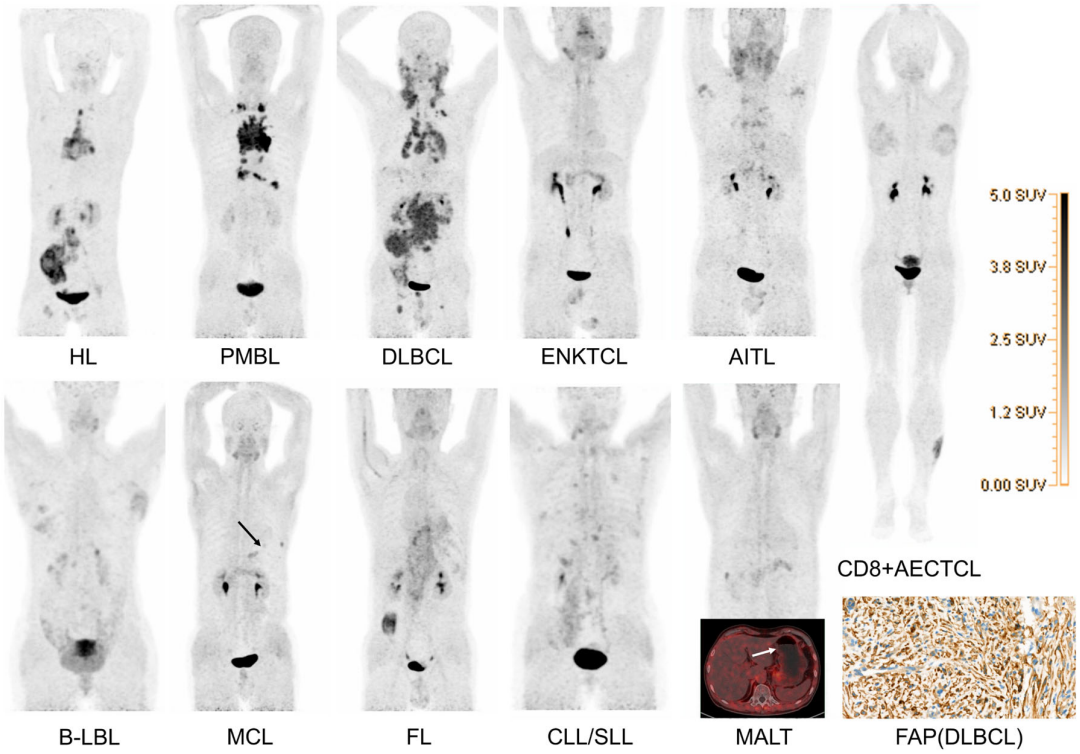

Maximum intensity projections (MIPs) of ^{68}Ga-FAPI PET/CT in patients of various histological subtypes (arrows in MIP and axial fusion image). HL, Hodgkin lymphoma; PMBL, primary mediastinal large B-cell lymphoma; DLBCL, diffuse large B-cell lymphoma; ENKTCL, extranodal NK/T-cell lymphoma; AITL, angioimmunoblastic T-cell lymphoma; $CD8^+$ AECTCL, cutaneous $CD8^+$ aggressive epidermotropic cytotoxic T-cell lymphoma; B-LBL, B lymphoblastic leukemia/lymphoma; MCL, mantle cell lymphoma; FL, follicular lymphoma; CLL/SLL, chronic lymphocytic leukemia/small lymphocytic lymphoma; MALT, mucosa-associated lymphoid tissue; FAP, fibroblast activation protein.

TABLE 1 Clinical Features of 73 Patients with Lymphoma

Parameters	**No. of patients (%)**
Gender	
Male	37 (50.68%)
Female	36 (49.32%)
Age	
>60 years	26 (35.62%)
≤60 years	47 (64.38%)
Treatment type	
Initial assessment	48 (65.75%)
Progressed	17 (23.29%)
Relapsed	8 (10.96%)
Lesion distribution	
Nodal only	15 (20.55%)
Extranodal, primary	19 (26.02%)
Both	39 (53.42%)
Histological subtype	
HL	11 (15.07%)
NHL	62 (84.93%)
DLBCL	34 (46.57%)
ENKTCL	5 (6.85%)
AITL	4 (5.48%)
PMBL	2 (2.74%)
BL	1(1.37%)
MCL	1 (1.37%)
B-LBL	1 (1.37%)
C-ALCL	1 (1.37%)
$CD8^+$ AECTCL	1 (1.37%)
FL	9 (12.33%)
MALT lymphoma	2 (2.74%)
CLL/SLL	1 (1.37%)

HL, Hodgkin lymphoma; NHL, non-Hodgkin lymphoma; DLBCL, diffuse large B-cell lymphoma; ENKTCL, extranodal NK/T-cell lymphoma; AITL, angioimmunoblastic T-cell lymphoma; PMBL, primary mediastinal large B-cell lymphoma; BL, Burkitt lymphoma; MCL, mantle cell lymphoma; B-LBL, B lymphoblastic leukemia/lymphoma; C-ALCL, primary cutaneous anaplastic large-cell lymphoma; $CD8^+$ AECTCL, cutaneous $CD8^+$ aggressive epidermotropic cytotoxic T-cell lymphoma; FL, follicular lymphoma; MALT, mucosa-associated lymphoid tissue; CLL/SLL, chronic lymphocytic leukemia/small lymphocytic lymphoma.

TABLE 2 SUV_{max} Values of Nodal and Extranodal Lymphoma Lesions

Lymphoma group	Histology	No. of patients	Nodal			Extranodal			*P*-value
			Average	Median	Range	Average	Median	Range	
Initial	HL	6	11.78 ± 4.03	11.8	7.3–18.1	7.20 ± 2.55	7.2	5.4–9.0	0.18
	DLBCL	22	8.52 ± 4.57	8.4	2.3–20.2	10.14 ± 4.33	10.9	3.7–17.1	0.08
	ENKTCL	3	5.40 ± 3.14	6.8	1.8–7.6	7.93 ± 1.12	8.2	6.7–8.9	0.29
	AITL	3	6.57 ± 2.40	6	4.5–9.2	2.4	2.4	N/A	N/A
	PMBL	2	18.40 ± 6.01	20.2	11.7–23.3	N/A	N/A	N/A	N/A
	BL	1	N/A	N/A	N/A	19.1	19.1	N/A	N/A
	B-LBL	1	2.3	2.3	N/A	6.5	6.5	N/A	N/A
	MCL	1	N/A	N/A	N/A	5.1	5.1	N/A	N/A
	FL	7	5.60 ± 2.71	5.4	1.7–9.8	7.95 ± 3.68	8.05	4.2–11.5	0.47
	MALT lymphoma	1	N/A	N/A	N/A	1.8	1.8	N/A	N/A
	CLL/SLL	1	5.9	5.9	N/A	4.5	4.5	N/A	N/A
	Total	48	8.35 ± 4.87	7.6	1.7–23.3	8.92 ± 6.08	8.2	1.8–19.1	0.11
Progressed	HL	3	9.63 ± 4.05	8.6	6.2–14.1	5.90 ± 5.44	3.7	1.9–12.1	0.29
	DLBCL	8	7.87 ± 1.89	8.7	4.3–9.7	9.40 ± 6.40	6.8	2.8–21.0	0.36
	$CD8^+$ AECTCL	1	N/A	N/A	N/A	8.4	8.4	N/A	N/A
	ENKTCL	1	N/A	N/A	N/A	7.5	7.5	N/A	N/A
	AITL	1	4.9	4.9	N/A	N/A	N/A	N/A	N/A
	MALT	1	4.9	4.9	N/A	5.6	5.6	N/A	N/A
	FL	2	5.5	5.5	4.3–6.7	12.3	12.3	N/A	N/A
	Total	17	7.49 ± 2.68	7.05	4.3–14.1	8.38 ± 5.23	7.15	1.9–21.0	0.60
Relapsed	HL	2	7.45 ± 3.75	7.45	4.8–10.1	6.75 ± 2.62	6.75	4.9–8.6	N/A
	DLBCL	4	5.67 ± 5.23	3.7	1.7–11.6	7.63 ± 3.68	6.65	4.4–12.8	0.96
	ENKTCL	1	N/A	N/A	N/A	8.7	8.7	N/A	N/A
	C-ALCL	1	N/A	N/A	N/A	5.2	5.2	N/A	N/A
	Total	8	6.38 ± 4.26	4.8	1.7–11.6	7.24 ± 2.80	6.65	4.4–12.8	0.95

HL, Hodgkin lymphoma; DLBCL, diffuse large B-cell lymphoma; ENKTCL, extranodal NK/T-cell lymphoma; AITL, angioimmunoblastic T-cell lymphoma; PMBL, primary mediastinal large B-cell lymphoma; BL, Burkitt lymphoma; N/A, not applicable; B-LBL, B lymphoblastic leukemia/lymphoma; MCL, mantle cell lymphoma; FL, follicular lymphoma; MALT, mucosa-associated lymphoid tissue; CLL/SLL, chronic lymphocytic leukemia/small lymphocytic lymphoma; $CD8^+$ AECTCL, cutaneous $CD8^+$ aggressive epidermotropic cytotoxic T-cell lymphoma; C-ALCL, primary cutaneous anaplastic large-cell lymphoma

TABLE 3 Size and SPD of Lymphoma Lesions

Histological subtype	No. of patients	Node size (cm)			SPD		
		Median	Average	Range	Median	Average	Range
HL	11	10.07	14.14 ± 13.22	2.53–47.23	27.13	41.44 ± 32.10	8.28–95.00
DLBCL	34	7.88	9.93 ± 12.12	3.55–58.83	35.43	43.51 ± 47.78	11.99–229.49
ENKTCL	5	2.53	2.29 ± 0.81	1.39–2.95	10.55	14.12 ± 7.86	7.09–24.47
AITL	4	4.60	4.58 ± 1.69	2.56–6.58	26.55	25.76 ± 18.36	2.56–47.36
PMBL	2	7.99	9.06 ± 4.99	3.55–19.35	39.61	38.02 ± 17.45	15.49–67.02
BL	1	N/A	N/A	N/A	18.18	18.18	18.18
MCL	1	N/A	N/A	N/A	15.89	15.89	15.89
B-LBL	1	2.71	2.71	2.71	43.03	43.03	43.03
C-ALCL	1	N/A	N/A	N/A	2.10	2.10	2.10
$CD8^+$ AECTCL	1	N/A	N/A	N/A	8.96	8.96	8.96
FL	9	5.40	8.23 ± 8.49	2.78–39.99	31.35	31.89 ± 18.40	5.56–70.88
MALT lymphoma	2	2.17	2.17	2.17	3.22	3.22 ± 1.57	2.11–4.33
CLL/SLL	1	8.84	8.84	8.84	32.6	32.6	32.6

SPD, sum of the product of the diameters; HL, Hodgkin lymphoma; DLBCL, diffuse large B-cell lymphoma; ENKTCL, extranodal NK/T-cell lymphoma; AITL, angioimmunoblastic T-cell lymphoma; PMBL, primary mediastinal large B-cell lymphoma; BL, Burkitt lymphoma; MCL, mantle cell lymphoma; N/A, not applicable; B-LBL, B lymphoblastic leukemia/lymphoma; C-ALCL, primary cutaneous anaplastic large-cell lymphoma; $CD8^+$ AECTCL, cutaneous $CD8^+$ aggressive epidermotropic cytotoxic T-cell lymphoma; FL, follicular lymphoma; MALT, mucosa-associated lymphoid tissue; CLL/SLL, chronic lymphocytic leukemia/small lymphocytic lymphoma.

SUPPLEMENT 1. Study flowchart of patient enrollment.